phys. stat. sol. (b) **234**, No. 3, 787–795 (2002)

Band Gap of Hexagonal InN and InGaN Alloys

V. Yu. Davydov[1]) (a), A. A. Klochikhin (a, b), V. V. Emtsev (a), D. A. Kurdyukov (a), S. V. Ivanov (a), V. A. Vekshin (a), F. Bechstedt (c), J. Furthmüller (c), J. Aderhold (d), J. Graul (d), A. V. Mudryi (e), H. Harima (f), A. Hashimoto (g), A. Yamamoto (g), and E. E. Haller (h)

(a) Ioffe Physico-Technical Institute, RAS, 19402 St. Petersburg, Russia

(b) Petersburg Nuclear Physics Institute, Russian Academy of Sciences, Gatchina, 188350 St. Petersburg, Russia

(c) Institut für Festkörpertheorie and Theoretische Optik, Friedrich-Schiller-Universität Jena, Max-Wien-Platz 1, 07743 Jena, Germany

(d) LfI University of Hannover, Schneiderberg 32, 30167 Hannover, Germany

(e) Institute of Solid State and Semiconductor Physics, Belarus Academy of Sciences, Brovki 17, 220072 Minsk, Belarus

(f) Department of Electronics and Information Science, Kyoto Institute of Technology, Matsugasaki, Sakyo-ku, Kyoto 606-8585, Japan

(g) Department of Electronics Engineering, Fukui University, Bunkyo, Fukui 910-8507, Japan

(h) University of California and Lawrence Berkeley National Laboratory, Berkeley, CA 94720, USA

(Received July 22, 2002; accepted October 1, 2002)

PACS: 71.20.Nr; 78.40.Fy; 78.55.Cr

A survey of most recent studies of optical absorption, photoluminescence, photoluminescence excitation, and photomodulated reflectance spectra of single-crystalline hexagonal InN layers is presented. The samples studied were undoped n-type InN with electron concentrations between 6×10^{18} and 4×10^{19} cm^{-3}. It has been found that hexagonal InN is a narrow-gap semiconductor with a band gap of about 0.7 eV, which is much lower than the band gap cited in the literature. We also describe optical investigations of In-rich $In_xGa_{1-x}N$ alloy layers ($0.36 < x < 1$) which have shown that the bowing parameter of $b \sim 2.5$ eV allows one to reconcile our results and the literature data for the band gap of $In_xGa_{1-x}N$ alloys over the entire composition region. Special attention is paid to the effects of post-growth treatment of InN crystals. It is shown that annealing in vacuum leads to a decrease in electron concentration and considerable homogenization of the optical characteristics of InN samples. At the same time, annealing in an oxygen atmosphere leads to formation of optically transparent alloys of InN–In_2O_3 type, the band gap of which reaches approximately 2 eV at an oxygen concentration of about 20%. It is evident from photoluminescence spectra that the samples saturated partially by oxygen still contain fragments of InN of mesoscopic size.

Introduction InN and $In_xGa_{1-x}N$ alloys have not been investigated thoroughly enough because of difficulties encountered in the growth of compounds with large size differences between cation and anion [1]. Recent progress in the growth techniques has made it possible to obtain perfect single-crystalline InN layers. Optical measurements

[1]) Corresponding author; Phone: +7 812 2479911; e-mail: valery.davydov@mail.ioffe.ru

© 2002 WILEY-VCH Verlag GmbH & Co. KGaA, Weinheim 0370-1972/02/23412-0787 $ 17.50+.50/0

have revealed that the fundamental absorption edge of these layers lies in the range from 0.9 to 1.1 eV and that there is a strong PL band in the range from 0.73 to 0.9 eV [2–4]. In this work we argue that the PL bands of nominally undoped InN samples show the typical features of the interband recombination in heavily doped n-type III–V crystals. Analysis of the PL band shape is used to show that the band gap of hexagonal InN crystals is close to 0.7 eV, which is lower than the value reported in the literature [5]. The influence of the Burstein-Moss effect on the optical absorption edge is studied. PL data of In-rich $In_xGa_{1-x}N$ alloys are presented. We also discuss the influence of post-growth treatment of InN crystals in order to reveal possible mechanisms of transformation of the crystal structure and the band gap variation.

Characterization of Samples Undoped InN epilayers were grown on (0001) sapphire substrates by different epitaxy methods [6–8]. A set of $In_xGa_{1-x}N$ layers ($0.36 < x < 1$) was grown by plasma assisted molecular beam epitaxy [3]. The composition and crystalline structure of the samples were characterized by a number of techniques. As evidenced by X-ray analysis, all the samples possess hexagonal symmetry and no traces of other polymorphes were detected. From symmetric (0002) and asymmetric ($11\bar{2}4$) Bragg reflections, lattice parameters c and a were found to be $c = 5.7039$ Å and $a = 3.5365$ Å, respectively. In the most perfect InN samples, the full widths at half maximum (FWHMs) for ω and θ-2θ scans at the (0002) reflection were typically in the ranges 250–300 arcsec and 50–60 arcsec, respectively. Polarized Raman spectra of InN and related alloys showed good agreement with the selection rules for the hexagonal symmetry. The phonon line widths of InN samples corresponded to that of a well-ordered crystal lattice. Atomic force microscopy measurements did not reveal any pronounced column structure of the samples studied. According to the Auger spectroscopic and Rutherford backscattering data, the oxygen concentration in the samples was about 1%. The Hall concentration of electrons n, ranged from 6×10^{18} to 4×10^{19} cm^{-3}, and the highest electron mobility μ was found to be $\sim$1900 cm^2 V^{-1} s^{-1} (for InN with $n = 8 \times 10^{18}$ cm^{-3}).

Luminescence and Absorption of Crystals with Large Electron Concentration The high energy PL band in heavily doped semiconductors of n-type results from recombination of degenerate electrons with photoholes near the top of the valence band. The shape of this PL band has two characteristic features. The first one is a high-energy wing of the band which exhibits an exponential decrease in the region of $(\hbar\omega - E_G(n)) \geq E_F$ due to a decrease in the electron population in accordance with the Fermi function

$$f(\hbar\omega - E_G(n) - E_F) = 1/[\exp\{(\hbar\omega - E_G(n) - E_F)/kT\} + 1]\,.$$

Here, $E_G(n)$ is a carrier-concentration-dependent parameter which approaches the band gap $E_G(n) \to E_G$ at vanishing concentration $n \to 0$, E_F is the Fermi energy of the degenerate electrons. The second feature is a low-energy wing of the PL band at $\hbar\omega < E_G(n)$, which typically shows the Urbach tail. This tail can overlap with the PL bands related to recombination of electrons with holes in deeper localized states.

Figure 1 shows the experimental and calculated luminescence bands in GaAs, InN, and GaN crystals with free electron concentrations of about 1×10^{19} cm^{-3}. The valence-conduction band diagram given in Ref. [9] leads to the following shape of the PL band in the energy region $\hbar\omega > E_G(n)$

$$I(\hbar\omega) \sim [\hbar\omega - E_G(n)]^{\gamma/2} f(\hbar\omega - E_G(n) - E_F)\,, \qquad (1)$$

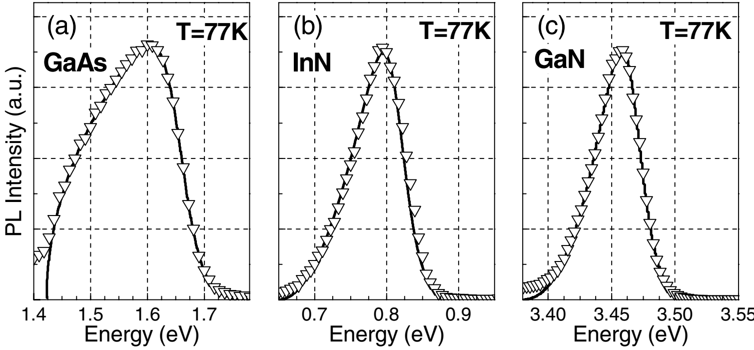

Fig. 1. Experimental and calculated luminescence bands in heavily doped GaAs (a), InN (b), and GaN (c) crystals with charge carrier concentrations of 1.1×10^{19}, 0.9×10^{19}, and $0.9 \times 10^{19}\,\mathrm{cm}^{-3}$, respectively. Points, experimental; curves, calculated

where $\gamma = 1$ if only vertical interband transitions are allowed, and $\gamma = 4$ if the momentum conservation law is completely broken as a result of the influence of defects and/or impurities on the hole or electron states. The experimental band shape in GaAs can be described well with $\gamma = 1$, whereas for GaN crystals γ equals 4. For InN γ increases from 2 to 4 with increasing concentration of free carriers.

High doping levels lead to changes in the interband absorption coefficient due to the Burstein-Moss effect. In analogy with Eq. (1), the interband absorption coefficient can be expressed as

$$\alpha(\hbar\omega) \sim [\hbar\omega - E_G(n)]^{\gamma/2}\,[1 - f(\hbar\omega - E_G(n) - E_F)]\,. \tag{2}$$

The absorption coefficient $\alpha(\omega)$ for InN samples measured at 300 K rapidly reaches values of the order of $\alpha(\omega) > 4 \times 10^4\,\mathrm{cm}^{-1}$ at the photon energy close to 1 eV. This

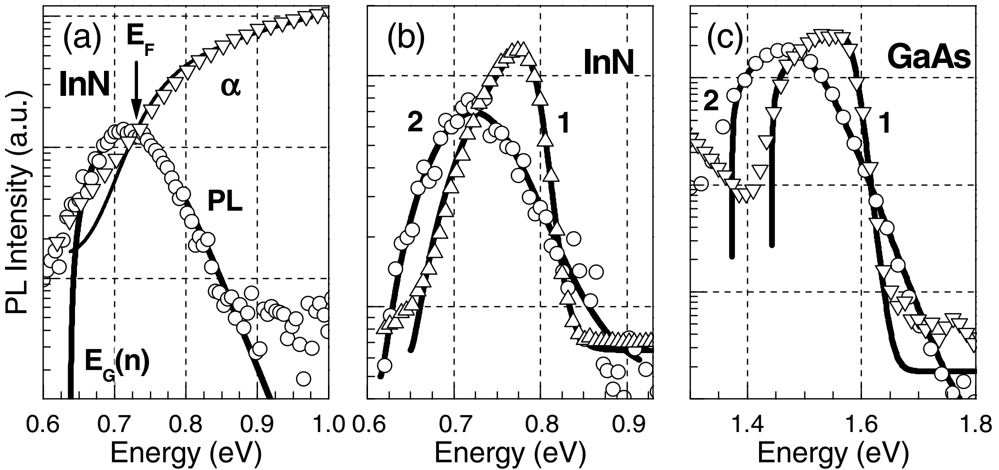

Fig. 2. a) Experimental and calculated luminescence bands and absorption coefficients in InN ($n = 6 \times 10^{18}\,\mathrm{cm}^{-3}$) at $T = 300$ K. Experimental and calculated luminescence bands at 77 (curves 1) and 300 K (curves 2): b) in InN ($n = 6 \times 10^{18}\,\mathrm{cm}^{-3}$) and c) in GaAs ($n = 4.3 \times 10^{18}\,\mathrm{cm}^{-3}$). Points, experimental; curves, calculated

high value of the absorption coefficient is typical of an interband absorption in direct-band-gap semiconductors.

The experimental luminescence spectrum and absorption coefficient of the InN sample with $n = 6 \times 10^{18}\ \text{cm}^{-3}$ at $T = 300$ K are presented in Fig. 2a together with corresponding curves calculated with Eq. (1) and Eq. (2). The same parameters are used in both expressions. It is seen that there is a good agreement between experimental and calculated data. Therefore, it can be concluded that the optical absorption and luminescence bands of InN crystals clearly have characteristics typical of interband transitions. Note that at large electron concentrations the absorption edge is well above the fundamental band gap (approximately by the value equal to the Fermi energy).

Temperature Dependence of the Luminescence Band Shape Modifications of the luminescence band shape with varying temperature are caused by redistribution of electrons over the energy levels in accordance with the Fermi function and also by the temperature shift of $E_G(n)$. The PL bands of InN and GaAs at 77 and 300 K are presented in Figs. 2b and 2c. A comparison of experimental spectra with calculated shapes allows us to find the temperature variation of parameter $E_G(n)$. The obtained temperature shift of $E_G(n)$ for GaAs crystal is about 70 meV, which agrees well with the band gap narrowing in this temperature interval. For the InN crystal, the shift is about 23 meV, which can also be related to the temperature-dependent band gap narrowing. Any anomalous temperature behavior of the PL band similar to that described in Ref. [4] was not observed in our experiments. The temperature shift of $E_G(n)$ for GaN crystals is consistent with literature data.

Concentration Dependence of PL Band and Absorption Coefficient The PL bands obtained at 77 K for the samples with different electron concentrations and the fitting curves obtained from Eq. (1) are shown in Fig. 3a. According to Hall measurements,

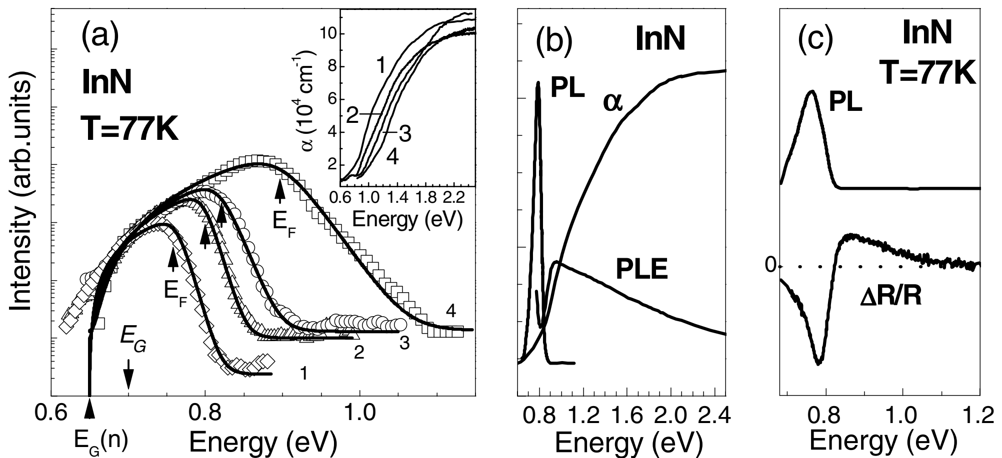

Fig. 3. a) Semilog PL spectra of InN layers with different charge carrier concentrations: $6 \times 10^{18}\ \text{cm}^{-3}$ (1), $9 \times 10^{18}\ \text{cm}^{-3}$ (2), $1.1 \times 10^{19}\ \text{cm}^{-3}$ (3), and $2.2 \times 10^{19}\ \text{cm}^{-3}$ (4). Points, experimental; curves, calculated. b) PLE spectrum measured at the PL band maximum on one of the samples, together with the PL and absorption spectra. c) PL and photomodulated reflectance spectra obtained on one of the InN samples

the free carrier concentrations in samples 1–4 are 6×10^{18}, 9×10^{18}, 1.1×10^{19}, and 2.2×10^{19} cm^{-3}, respectively. The temperature estimated from the exponential slope of the high-energy wing of the PL band is close to the measured temperature, except for InN sample 4. This discrepancy is probably due to the large layer inhomogeneity for the sample with the highest carrier concentration.

The Fermi energies E_F estimated from these PL spectra are 95, 147.5, 167.5, and 245 meV in samples 1 to 4, respectively. Assuming an isotropic electron band, E_F as a function of electron concentration n/n_0 ($n_0 = 1 \times 10^{18}$ cm^{-3}) is given by

$$E_F = 3.58\,(m_0/m^*)\,(n/n_0)^{2/3}\ \text{meV}\,. \tag{3}$$

Comparison of the Fermi energies of GaAs, InN, and GaN crystals (see Fig. 1) leads to the conclusion that the electron effective mass in InN lies between those in GaAs and GaN. The electron concentrations calculated from the Fermi energies based on the assumption of an effective mass of $m^* = 0.1\,m_0$ are in good agreement with the Hall data. The shift of the optical absorption edge due to the Burstein-Moss effect for the same samples is shown in the inset of Fig. 3a. It is seen that the shifts are considerable in this concentration range due to the large values of E_F.

As it follows from Eq. (1) the low energy onset of the PL fitting curves defines $E_G(n)$. It has been found that $E_G(n)$ is weakly dependent on the electron concentration and close to 0.65 eV.

Photoluminescence Excitation and Photomodulated Reflectance Spectra The PLE spectrum measured at the PL band maximum together with the PL and absorption spectra for one of the samples are shown in Fig. 3b. It can be seen that the PLE spectrum behaves similarly to the absorption spectrum up to some energy. However, at the energy $\hbar\omega_{max}$, far from the absorption saturation, it displays an abrupt kink, and its intensity starts to fall. Such a behavior of the PLE spectrum can be understood if one takes into account that at energies $E < \hbar\omega_{max}$ the photons create holes in the localized states, and at $E > \hbar\omega_{max}$ the production of mobile holes dominates. When two mobile particles – an electron and a hole – are produced, the probability of formation of a separated e–h pair and, hence, the probability of nonradiative relaxation of each particle increases sharply. As a result, the PLE efficiency substantially decreases. The PLE results are correlated with those of absorption and PL. The three spectroscopies give nearly the same gap energy.

Figure 3c displays the PL and photomodulated reflectance (PR) spectra obtained for one of the InN samples. The zero point of the PR spectrum is close to the energy $(\hbar\omega - E_G(n)) = E_F$, and the shape of the PR spectrum indicates that the Fermi distribution of electrons is affected by photomodulation.

Concentration Dependence of $E_G(n)$ $E_G(n)$ as a function of charge carrier concentrations for GaAs, InN, and GaN crystals given in Fig. 4. It shows a nearly linear dependence on $n^{1/3}$ where n was estimated from Eq. (3).

In this case the shift of $E_G(n)$ ($\Delta E_G(n)$) can be explained by a decrease in the exchange interaction energy [10], which in the framework of perturbation theory can be written as

$$E_{ex}(n) = -e^2/2 \sum_{\sigma,p,p' \le pF} \int d^3r \int d^3r' \psi^*_{\sigma,p}(\mathbf{r}) \psi^*_{\sigma,p'}(\mathbf{r}) \psi_{\sigma,p}(\mathbf{r}') \psi_{\sigma,p'}(\mathbf{r}') / |\mathbf{r} - \mathbf{r}'|\,.$$

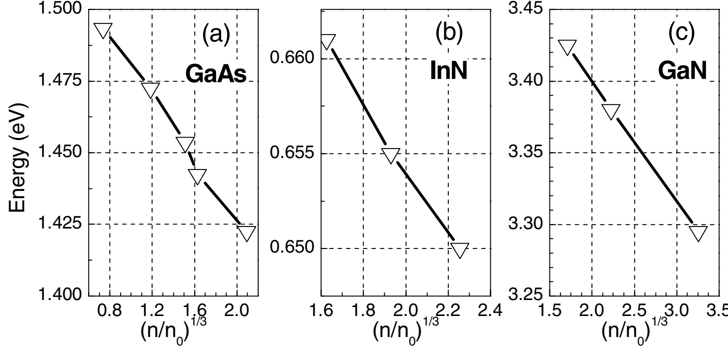

Fig. 4. Parameter $E_G(n)$ versus the free carrier concentrations for GaAs (a), InN (b), and GaN (c) crystals

In the effective mass approximation, for an isotropic electron band, the shift is

$$\Delta E_G(n) = -\left(\frac{81}{\pi}\right)^{1/2} \frac{e^2 n^{1/3}}{2} = -106(n/n_0)^{1/2}\ \text{meV}\,,$$

where e and σ are the charge and spin of an electron. The value of $\Delta E_G(n)$ in this approximation is a universal function of the electron concentration. The individual characteristics of a crystal appear only if the Bloch wave functions like $1/\sqrt{V} u_{\sigma,p}(\mathbf{r}) \exp(i\mathbf{pr})$ are used in calculations of the exchange energy. As a consequence of structure of the Hartree-Fock exchange energy, the overlapping integrals of Bloch factors $\left(u^*_{\sigma,p}(\mathbf{r})\, u_{\sigma,p'}(\mathbf{r})\right)$ appear in calculations. These integrals are less than unit and, therefore, the effective mass approximation gives an upper limit of $\Delta E_G(n)$.

The slopes of the experimental curves in Fig. 4 are smaller than the theoretical value of 106 meV and are equal to 54, 84, and 17 meV for GaAs, GaN, and InN crystals, respectively. The observed behavior of $E_G(n)$ of InN largely deviates from the theoretical value obtained in the effective mass approximation and, hence, its description has to be improved.

An extrapolation of $E_G(n)$ to $n \to 0$ gives the estimate of the true band gap of InN $E_G = 0.69$ eV. The value of $E_G \sim 0.69$ eV is slightly smaller than that suggested by calculations [11].

Optical Spectra of $In_xGa_{1-x}N$ Layers The InN band gap can also be estimated from optical spectra of $In_xGa_{1-x}N$ alloys in the limit $x \to 1$. Figure 5a shows the PL and absorption spectra for some In-rich alloys ($0.36 < x < 1$). It is seen that the PL bands and the absorption edge shift toward higher energies as x decreases. Like in InN, the maximum of the PL band in alloys is redshifted from the absorption edge by the value of about one half of the FWHM of the PL band. This shift is consistent with the estimate of the Burstein-Moss effect in our alloys with electron concentrations in the $4–7 \times 10^{19}\ \text{cm}^{-3}$ range. A considerably larger Stokes shift of the PL bands in In-rich alloys was observed in Ref. [15].

Similar to InN, analysis of the PL band shape using Eq. (1) gives the value of $E_G(n)$ for alloys. Figure 5b depicts $E_G(n)$ for In-rich alloys studied in this work as a function of alloy composition. The composition was estimated, according to the Vegard's law, from the

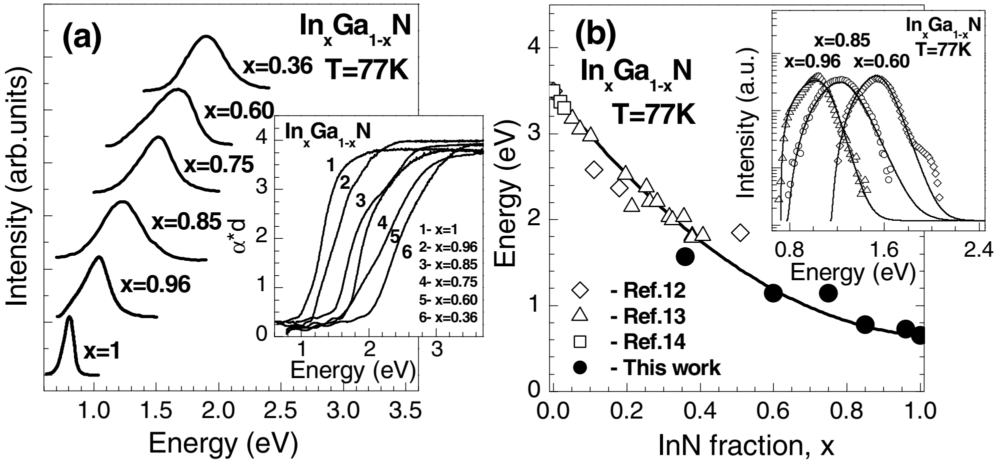

Fig. 5. a) PL spectra and absorption edges in In-rich $In_xGa_{1-x}N$ layers; b) $E_G(n)$ estimated for the In-rich alloys studied in this work, and the positions of PL band maxima in Ga-rich alloys taken from Refs. [12–14] as a function of composition. The inset shows semilog PL spectra and calculated curves, obtained using Eq. (1) for the most perfect alloys: $x = 0.96$ (1), $x = 0.85$ (2), and $x = 0.75$ (3)

lattice constant c obtained from X-ray measurements. This figure also presents the position of the PL band maxima taken from the literature for Ga-rich $In_xGa_{1-x}N$ alloys. The experimental points in Fig. 6b are fitted by a smooth curve $E_G = 3.493 - 2.843\,x - b\,x\,(1-x)$ with the bowing parameter $b = 2.5$ eV. Indeed, the data obtained from PL spectra of In-rich $In_xGa_{1-x}N$ layers confirm the small value of the InN band gap.

The Wide-Gap InN-Based Samples In attempts to understand the reasons for the striking discrepancy between our data on the band gap with those cited in the literature, we studied several samples, which were claimed to be hexagonal InN with band gaps in the region of 1.8–2.1 eV. The samples were grown by different techniques on different substrates but all the samples have some common features. The transmission spectra of these samples are strongly affected by plasma reflection in the IR region pointing to very high charge carrier concentrations, up to 6×10^{20} cm^{-3}. The samples have a polycrystalline structure as deduced from very wide X-ray rocking curves. The broad features of Raman spectra reproducing the phonon-density-of-states function (DOS) are observed in contrast to the sharp polarized lines in our single crystalline samples. Therefore, both the X-ray and Raman data suggest the presence of structural de-

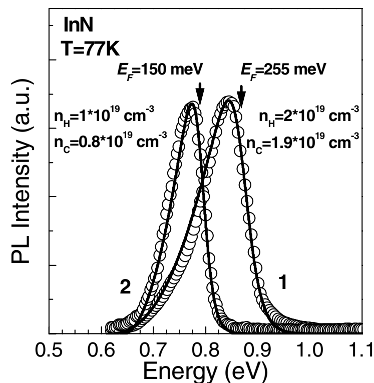

Fig. 6. PL spectra in InN samples before (curve 1) and after (curve 2) annealing in vacuum

fects in high concentrations. The chemical composition analysis by Auger spectroscopy and Rutherford backscattering technique revealed very high oxygen contents in wide-gap samples, up to 20 at%, much higher than in our samples. It can be assumed that it is oxygen that is responsible for a high concentration of defects. In this case an increase of the band gap in wide-gap samples can be caused by formation of oxynitrides, which have much larger band gaps than that of InN. The Burstein-Moss effect in polycrystalline samples with high charge carrier concentrations may also be responsible for sizable changes in the band gap.

Post-Growth Treatment of InN Samples Some of the samples were subjected to annealing at 490 °C for 5 hours in vacuum. As can be seen from Fig. 6, the treatment results in a substantial decrease in the PL band FWHM and increase in the high-energy wing slope. This transformation suggests that the electron concentration decreases, and the distribution of the electron density over the sample becomes more homogeneous. Hall measurements revealed that the annealing results in a decreasing charge carrier concentration, too.

Annealing in an oxygen environment leads to formation of optically transparent oxynitrides whose band gap depends on the oxygen concentration in the sample and approaches 2 eV at oxygen concentrations of about 20%. The adsorption and luminescence spectra in such samples demonstrate a wide Urbach-like tail of localized states spreading over the entire region below the band edge. X-ray and Raman measurements revealed the formation of alloys of the $InN-In_2O_3$ type. From the luminescence spectra it is evident that the samples saturated partially with oxygen still contain InN fragments of mesoscopic size. The InN PL band in such samples is slightly shifted towards high energies, which can be attributed to the size quantization effect. The final stage of oxydation is the formation of In_2O_3 crystals.

Summary To summarize, analysis of optical absorption, PL, PLE and photoreflectivity data obtained on single-crystalline hexagonal InN leads to the conclusion that the true band gap of InN is $E_G \sim 0.7$ eV. This finding is supported by optical studies of In-rich $In_xGa_{1-x}N$ alloys. Our studies of InN samples with E_G of 1.8–2.0 eV revealed that the increased band gap may be due to the formation of oxynitrides, which have much larger band gaps than that of InN.

Acknowledgements The authors are grateful to Prof. R. A. Suris, Prof. S. A. Permogorov, and Prof. B. V. Novikov for fruitful discussions. We thank A. V. Sakharov, V. A. Kapitonov, A. N. Smirnov, D. S. Sizov, N. V. Kryzhanovskaya, and V. V. Mamutin for their assistance in measurements and MBE growth. The authors thank Prof. T. Inushima and Dr. K. S. Butcher for the sample exchanges. This work is supported by the Programs “Lowdimensional Quantum Structures” and “Nanostructures”, and CRDF (grant No. RP1-2258).

References

[1] S. Nakamura and G. Fasol, The Blue Laser Diode, Springer, Berlin 1997.

[2] V. Yu. Davydov, A. A. Klochikhin, R. P. Seisyan, V. V. Emtsev, S. V. Ivanov, F. Bechstedt, J. Furthmüller, H. Harima, A. V. Mudryi, J. Aderhold, O. Semchinova, and J. Graul, phys. stat. sol. (b) **229**, 1 (2002).

[3] V. Yu. Davydov, A. A. Klochikhin, V. V. Emtsev, S. V. Ivanov, V. V. Vekshin, F. Bechstedt, J. Furthmüller, H. Harima, A. V. Mudryi, A. Hashimoto, A. Yamamoto, J. Aderhold, J. Graul, and E. E. Haller, phys. stat. sol. (b) **230**, 4 (2002).
[4] J. Wu, W. Walukiewicz, K. M. Yu, J. W. Ager III, E. E. Haller, H. Lu, W. J. Schaff, Y. Saito, and Y. Nanishi, Appl. Phys. Lett. **80**, 3967 (2002).
[5] T. L. Tansley and C. P. Foley, J. Appl. Phys. **59**, 3241 (1986).
[6] V. V. Mamutin, V. A. Vekshin, V. Yu. Davydov, V. V. Ratnikov, V. V. Emtsev, and S. V. Ivanov, phys. stat. sol. (a) **176**, 247 (1999).
[7] J. Aderhold, V. Yu. Davydov, F. Fedler, H. Klausing, D. Mistele, T. Rotter, O. Semchinova, J. Stemmer, and J. Graul, J. Cryst. Growth **222**, 701 (2001).
[8] E. Kurimoto, H. Harima, A. Hahimoto, and A. Yamamoto, phys. stat. sol. (b) **228**, 1 (2001).
[9] E. Burstein, Phys. Rev. **93**, 632 (1954).
[10] D. Pines and P. Nozieres, The Theory of Quantum Liquids, W. A. Benjamin, inc., New York 1966.
[11] F. Bechstedt, J. Furthmüller, M. Ferhat, L. K. Teles, L. M. R. Scolfaro, J. R. Leite, V. Yu. Davydov, O. Ambacher, and R. Goldhahn, phys. stat. sol. (b) (2002), to be published.
[12] M. H. Kim, J. K. Cho, I. H. Lee, and S. J. Park, phys. stat. sol. (a) **176**, 269 (1999).
[13] K. P. O'Donnell, J. F. W. Mosselmans, R. W. Martin, S. Pereira, and M. E. White, J. Phys.: Condens. Matter **13**, 6977 (2001).
[14] A. Klochikhin, A. Reznitsky, L. Tenishev, S. Permogorov, W. Lundin, A. Usikov, S. Sorokin, S. Ivanov, M. Schmidt, H. Kalt, and C. Klingshirn, Nanostructures: Physics and Technology, Ioffe Institute, St. Petersburg 2001 (p. 554).
[15] J. Wu, W. Walukiewicz, K. M. Yu, J. W. Ager III, E. E. Haller, H. Lu, and W. J. Schaff, Appl. Phys. Lett. **80**, 4741 (2002).